JOURNAL OF MATERIALS SCIENCE **40** (2005) 2179–2184

The effect of gas flow rate on the evolution of the surface oxide on a molten low carbon Al killed steel

Y. WANG, S. SRIDHAR
Department of Materials Science and Engineering, Carnegie Mellon University, Pittsburgh, PA 15213, USA

The oxide phase formation on a molten Al killed low carbon steel surface under a flowing Ar atmosphere with an oxygen partial pressure of $Po_2 = 1\text{–}5 \times 10^{-5}$ atm has been visualized with a Confocal Scanning Laser Microscope (CSLM) equipped with a gold image furnace. In this study, the effect of gas flow rate variation (170–300 cm^3/min) on the oxide evolution under isothermal conditions of 1600°C was investigated. Al_2O_3, rather than the thermodynamically stable phase $FeAl_2O_4$, was found to precipitate under all the experimental conditions studied and the apparent rate of evolution was found to increase with increasing gas flow rate. The oxide evolved as a network that started from the container wall and grew towards the crucible center. At low flow rates the growth was a result of primarily crystal growth resulting in distinctly dendritic crystals. As the flow rate was increased, growth due to the attachment of discrete inclusions to the advancing front was observed which resulted in a final oxide network that constituted of smaller facetted particles. In the latter case, the transport of the individual inclusions to the advancing front could be caused by surface Marangoni flow due to gradients in both temperature and dissolved oxygen concentration.

1. Introduction

Reoxidation of molten steel surface as a result of unwanted reaction between reactive elements in melt with air, is a cause of exogenous inclusions that can get entrained into the melt and lead to lowering product quality [1]. Melt reoxidation with air is likely to happen primarily [2] at refractory joints and nozzles between vessels in the steelmaking and continuous casting process and can lead to deposits on the walls that results in clogs that prevent a uniform steel melt flow which degrade process control [3]. Sasai [4, 5] studied how reoxidation caused by air leads to Al_2O_3 buildup in the tundish nozzle, and found that during stable casting modest reoxidation resulted solely from oxidation by air on the tundish bath surface, whereas during teeming the reoxidation increased fivefold and was caused primarily by oxidation at the tundish inlet. Gas phase mass transfer to a melt has been extensively studied and documented in literature [e.g. 6]. Sasai and Mizukami [7] developed models based on experimental results [8, 9] to predict the melt reoxidation rates in the tundish based on gas phase mass transfer through the tundish inlet and top covering tundish powder. Precipitation of the oxide phase follows a chemical reaction between metallic elements in the melt (unreacted deoxidation reactants such as Al, Si or Ca and/or Fe) and oxygen dissolved in the melt, and the thermodynamic basis of this reaction is essentially similar to the well studied [10] deoxidation equilibrium that takes place in the ladle.

Besides the aforementioned problems associated with process control, oxide inclusion defects are known [11] to be an important factor that affects the mechanical properties of the final steel products. Large macro-inclusions are known to be especially detrimental [2] to properties but on the other hand, inclusion removal by flotation through the bath, following Stokes' law, is favored when the inclusion size is large. Whether large inclusion clusters in the melt are desired or not, it is important to be able to predict the size evolution with time. Oxide size evolution occurs by one or both of two mechanisms, crystal growth [12] and agglomeration [13]. In the case of crystal growth of Al_2O_3 in steel melts, a recent study [14] indicates that high supersaturation leads to the formation of spherical particles, or when impurity adsorption took place plate-like particles. Non-uniform supersaturation over the particle surface leads to dendrite formation. Under low supersaturation, near equilibrium conditions, the particles were found to become facetted. When simultaneous growth and sintering occurred, the particles assumed octahedral forms.

Agglomeration and sintering, is driven by surface tension reduction which is highly favored in the case of Al_2O_3 in steel due to non-wetting conditions. It is caused by collisions in the melt. When a gas phase is present at free surfaces or gas bubbles, clustering can occur at short separation distances for solid Al_2O_3 through attractive forces caused by capillary depression of the melt meniscus [15]. Yin *et al.* [15–18]

TABLE I Sample composition of the steel (in wt.%) investigated

C	Si	Mn	S	P	Al (total)	Al (soluble)
0.062	0.003	0.32	0.011	0.012	0.039	0.035

successfully quantified the clustering behavior of inclusions on melt surfaces by using a confocal scanning laser microscope (CSLM) equipped with a gold image furnace. In this paper, *in-situ* observations through a CSLM combined with SEM-EDS is used to visualize the growth of Al_2O_3 at steel/gas interfaces due to reoxidation. The effects of gas flow rate is investigated and the results are discussed in terms of kinetics and surface fluid flow.

2. Materials and experimental methods

2.1. Materials

The steel used in this study was a low-carbon Al-killed steel obtained as a solidified lollypop from the conventional ladle furnace installed in the steelmaking shop of Siderar (San Nicolas, Argentina) after Al-deoxidation but before calcium treatment. Chemical composition for this steel grade measured with an emission spectrometer is listed in Table I. The soluble Al content is obtained by subtracting the Al combined with oxygen as oxides determined by the spectrometer, from the total Al content.

The natural inclusions found in this sample were examined by SEM-EDS to be Al_2O_3-MgO-CaO, while about 90% of the inclusions are pure Al_2O_3. The size and compositional distribution of inclusions encountered in this grade have been quantified by a Scanning Electronic Microscope (SEM) equipped with an Energy Dispersive Spectroscopy (EDS) system. An automatic particle analyzer software was employed to evaluate the number, size and composition of nonmetallic inclusions in a relatively large area of the steel sample (140 mm^2), and the results are shown in Fig. 1.

2.2. Experimental methods

The experimental approach undertaken in this study was to observe the reoxidation process on the surface of molten steel sample by using a high temperature confocal scanning laser microscope (CSLM) under controlled temperatures and atmosphere, and analyze the inclusions after the experiments with a scanning electron microscope (SEM) combined with energy dispersive spectrometer (EDS).

The CSLM utilizes a confocal optics and a laser (He-Ne laser with wave-length of 632.8 nm) light source, and when equipped with a gold image high temperature furnace, it is capable of real time 3D imaging of uneven surfaces such as a high temperature liquid/gas interface. The high speed scanning by the acousto-optical device (AOD) enables confocal images to be obtained at a rate of several hundred times faster than with the standard confocal microscope. With this system, it is possible to collect a series of images of in-focus layers and combine them into a single three-dimensional image in real time. Therefore, the CSLM is ideally suited for *in-situ* study of fluid flow, chemical reaction and phase transformation.

A high temperature gold image furnace, schematically shown in Fig. 2a, is used to melt samples by reflecting the light of a halogen bulb on the sample. The steel sample was placed in cylindrical Al_2O_3 crucible of 5.5 mm diameter and 3 mm height which was inserted in a Pt/ Al_2O_3 sample holder, shown in Fig. 2b. The sample holder is equipped with a B-type thermocouple which is used to monitor the temperature in the hot zone. The temperature of the sample surface was calibrated by measuring the melting points of pure Ni and Cu in the same condition. The oxygen partial pressure of both the inlet and outlet gas was monitored with a solid state stabilized ZrO_2 based oxygen probe.

In order to characterize the morphology and composition of inclusions formed during reoxidation, a scanning electron microscope (SEM) combined with

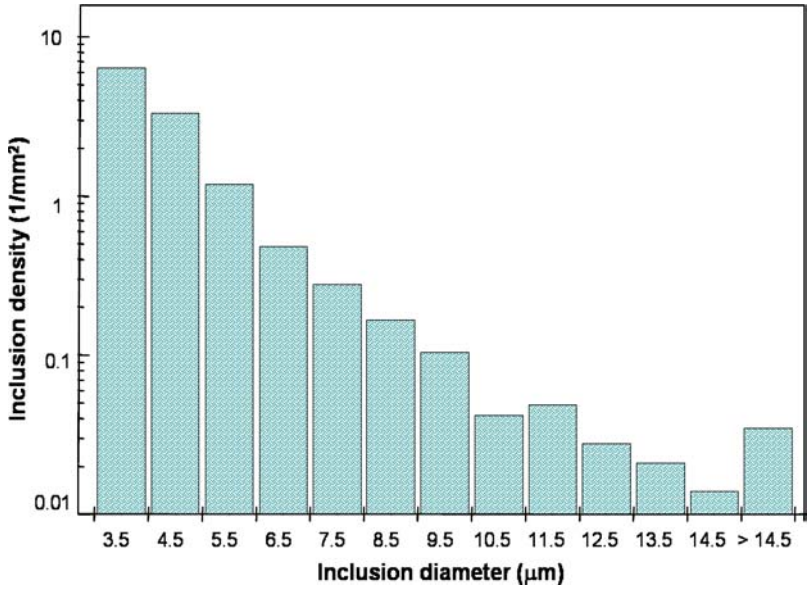

Figure 1 Inclusion size distribution.

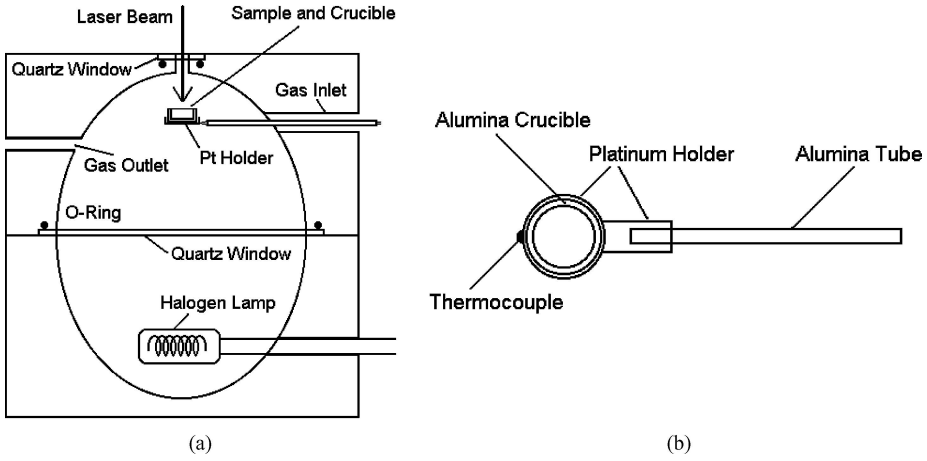

Figure 2 Schematic diagram of (a) high temperature gold image furnace, and (b) sample holder configuration (after Wang *et al.* [19]).

energy dispersive spectrometer (EDS) (PHILIPS XL-30) was utilized to analyze the samples after the CSLM experiments.

2.3. Procedure

The CSLM visualization experiments were performed according to the following procedure: (i) a clean atmosphere in the furnace chamber with sample was established by several sequences of vacuum purging and backfilling with pure Ar, (ii) the sample was then melted and maintained at the experimental temperature, (iii) after a time delay, the reoxidation was observed on the sample surface and the subsequent inclusion evolution was detected. The time delay is essentially the time period passed between reaching the experimental temperature and until experimental observation of a continuously growing oxide phase was observable. The time of detection of this event is limited by the in-ability to focus on the entire sample and the resolution limit of the microscope. Nevertheless, the measured time delay was for a given set of condition quite repeatable between experiments and exhibited a trend with respect to gas flow rate. The time delay was therefore considered as a rough indication of an incubation time for appreciable oxide nucleation to take place.

The observed real-time images were continuously exported to a video recorder and the inclusion size and growth rate were analyzed with an image analysis software NIH, which was developed at the National Institutes of Health.

3. Results and discussion

In this study, the reoxidation of low-carbon Al-killed steel was investigated under different experimental conditions. Temperature was maintained at 1600°C. Gas flow rates, in the range 170–300 cm^3/min were investigated. These limits were due to experimental difficulties. At flow rates below 170 cm^3, the difference between the inlet and outlet P_{O_2} was significant due to oxygen absorption and/or reaction with the melt which caused an uncertainty to the atmosphere over the melt. At flow rates above 300 cm^3/min, on the other hand, the gas was found to cool the sample, resulting in surface solidification.

During the experiments, the surface oxide would evolve in the following manner. Firstly, after a distinct time delay a few individual oxide inclusions would form and subsequently move towards the container wall, likely due to the fluid flow caused by the curved shape of the melt surface and Marangoni flow due to the 4 K/mm thermal gradient between the crucible walls and crucible center. Thereafter an oxide phase could be seen to grow, starting from the agglomerated oxides at the wall, and proceed towards the center. The time delay, oxide growth rate (measured as surface coverage rate) and morphology were characterized for each experiment and after cooling to room temperature, the oxide chemistry and scale thickness were determined with SEM-EDS. The experimental conditions and their corresponding results for each CSLM experiment and subsequent characterization are summarized in Table II.

The thermodynamically predicted phases were computed by using the software FactSage [20] and the

TABLE II Reoxidation experiments that were performed under different conditions

#	T (°C)	Flow rate (cm^3/min)	P_{O_2}(inlet) (atm)	P_{O_2}(outlet) (atm)	Time delay (min)	Coverage rate (%/s)	Oxide phase	Thickness (μm)
1	1600	105	1.3×10^{-4}	9.1×10^{-5}	65	0.0051	Al_2O_3	2
2	1600	170	7.0×10^{-5}	4.0×10^{-5}	44	0.0193	Al_2O_3	2
3	1600	225	4.0×10^{-5}	3.2×10^{-5}	33	0.0304	Al_2O_3	2
4	1600	300	2.8×10^{-5}	2.2×10^{-5}	28	0.0467	Al_2O_3	2

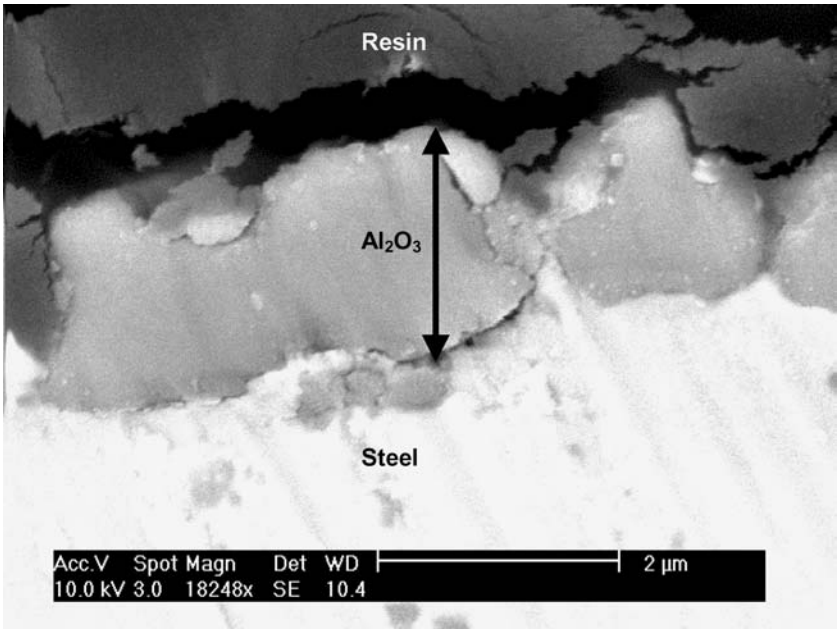

Figure 3 SEM-micrograph of the oxide and steel interface.

results showed that, due to the relatively high P_{O_2} in the inlet gas, solid $FeAl_2O_4$ with liquid FeO would be thermodynamically stable. When analyzing the surface oxides formed under SEM after the CSLM experiment, however, they were found to be Al_2O_3 in all cases. This is likely due to the fact that equilibrium is not reached, i.e., a mass balance revealed that the total amount of oxygen that the melt is exposed to during the experimental time is not enough to consume all the dissolved Al.

The oxides were in all cases 2 μm thick. A typical case of a steel/oxide scale interface is shown in Fig 3. EDS analysis showed that the scale was constituted of Al_2O_3. EDS line scans were also carried out to determine whether any Al or O compositional differences could be detected in the steel near the oxide scale but no gradients were detected. The fact that the oxide layer remained constant in all experiments, suggests that the reaction is limited to the surface regime. Under the experimental conditions and time periods studied, this suggests that oxygen does not penetrate into the melt but instead reacts with Al present at or near the surface. Thus, oxygen availability appears to be the rate limiting step.

From Table II, it can be seen that the gas flow rate has a considerable effect on the reoxidation onset and rate. The gas flow rate also influenced the morphology of the evolving oxide phase. Fig. 4 lists the CSLM images for Al_2O_3 growing at three different gas flow rates while the temperatures all at 1600°C, along with the SEM results showing the final phase morphology. At low flow rates, a dendrite like morphology was observed, whereas at higher rates the oxide phase changed successively into what appeared as agglomerates of particles. The observation that some facetted particles formed at flow rates below 225 cm^3/min agrees with literature [14] documenting that octahedral particles were observed when simultaneous growth and sintering occurred.

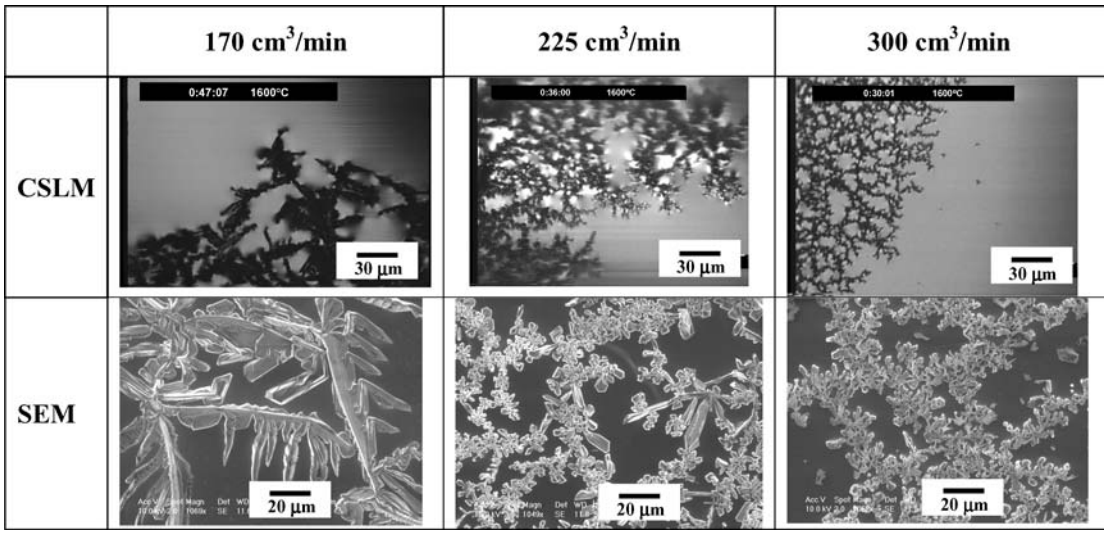

Figure 4 CSLM images of Al_2O_3 growth and the corresponding SEM morphology for Al_2O_3 formed under different gas flow rates at 1600°C. The time bars for the CSLM images represent hours:minutes:seconds.

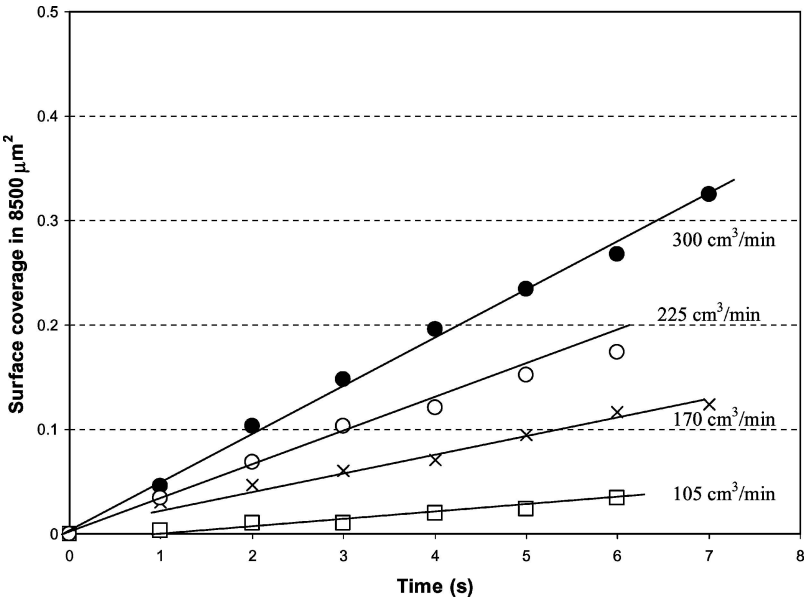

Figure 5 The effect of gas flow-rate on the fraction of a 8500 μm^2 surface covered by alumina.

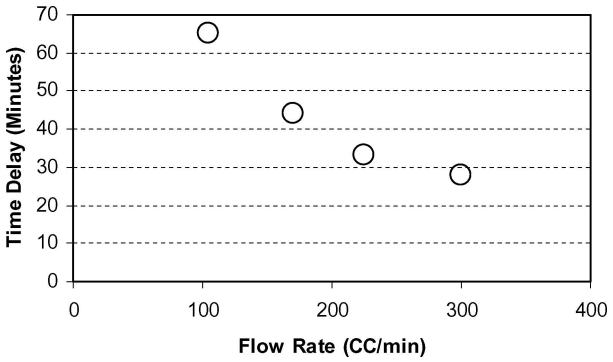

Figure 6 Time delay as a function of Ar gas flow rate at 1600°C.

Fig. 5 shows the fraction of surface coverage by the oxides on an area of 8500 μm^2 as a function of time under Ar gas flow rate of 105, 170, 225 and 300 cm^3/min. The rates can be seen to be linear in all cases and decrease with decreasing flow rate. The effect of flow rate on the apparent time delay for the onset of growth is shown in Fig. 6 where it can be seen that the time delay increases with decreasing flow rate.

Table III summarizes the observations of the reoxidation products in Fig. 4. At low gas flow rates, nucleation is low and oxides grow as a result of crystal growth. The crystal growth appears to be unstable, possibly as a result of the fast rate due to the large driving force, and as a result dendrites without crystallographic planes are formed. Increasing the flow rate seem to encourage the nucleation of additional oxide particles ahead of the front. This results in the lowering of the driving force and thus faceted crystals are formed.

As the flow rate was increased and as a result nucleation rate was increased, newly formed particles were observed to flow towards the oxide front growing from the crucible wall. An example is shown in the sequence of images in Fig. 7. As can be seen in the time bar in Fig. 7, the velocity of the inclusion approaching the cluster front is quite rapid, and considering that the frames are 1/30 s apart, appears to move at $v > 400$ μm/s.

The flow of newly nucleated oxides towards the advancing front is likely due to Marangoni flow as a result of gradients in temperature and dissolved oxygen analogous to what Kimura *et al.* [21] reported for the behavior of inclusions ahead of advancing steel solidification fronts. This is schematically described in Fig. 8.

A thermal gradient of approximately 4K/mm results in a high surface tension as one approaches the crucible wall. This is under the assumption that the overall dissolved oxygen content is sufficiently high to maintain a positive temperature dependency of γ. If the advancing front establishes a local Al_2O_3/$\underline{O}$ equilibrium, a concentration gradient is established resulting in a high surface tension near the advancing front compared to the center of the melt surface. Hence, both the thermal and dissolved oxygen gradients could contribute to Marangoni flow towards the advancing front which could explain the transport of newly nucleated oxides towards the advancing front. At present the contributions from the solute gradient can not be quantified since the CSLM samples where found to be to small for accurate oxygen analysis through spectroscopic methods.

TABLE III The observed oxide morphology at different gas flow rates

Flow rate	170 cm^3/min	225 cm^3/min	300 cm^3/min
Nucleation amount	No additional nucleation	38/mm^2.s	729/mm^2.s
Precipitate morphology	Dendrite	Dendrite and facetted crystals	Facetted crystals
Approximate precipitate size	60 μm (primary dendrite arm)	2 μm diameter faceted crystals	3 μm diameter faceted crystals

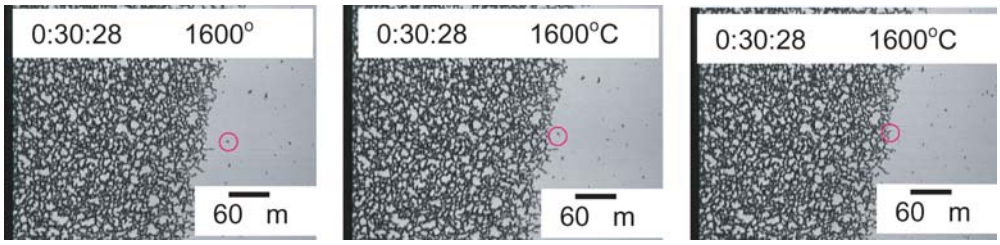

Figure 7 Sequence of CSLM images of the inclusion attachment to the front for flow rate of 300 cm^3/min at 1600°C. The time bars for the CSLM images represent hours:minutes:seconds and time interval between the images is 1/30 s.

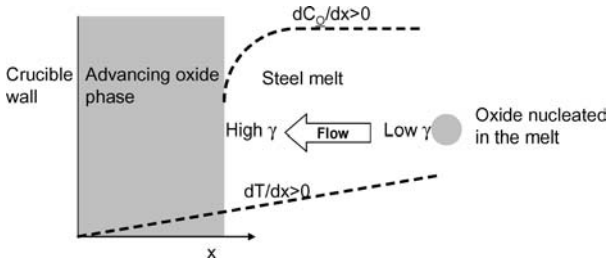

Figure 8 Schematic illustration of the direction of Marangoni flow.

4. Conclusions

Formation of Al_2O_3 on the surface of molten Al-killed low carbon steel was studied through direct observation in a high temperature confocal scanning laser microscope. Gas flow rates of 170–300 cm^3/min at 1600°C were investigated. The results indicated that:

1. The oxide phase formed on the melt surface was 2 μm thick and was constituted in all cases of Al_2O_3 and no $FeAl_2O_4$ or FeO was found.
2. The morphology of the oxide changed gradually from distinctly dendritic at low gas flow rates to aggregates as the flow rate was increased.

Acknowledgements

Financial support from the National Science Foundation under the CAREER grant DMR 0348818 is greatly acknowledged.

References

1. J. W. FARRELL, P. J. BILEK and D. C. HILTY, in Electric Furnace Proceedings (TMS-AIME, Pittsburgh,1970), Vol. 28, p. 64.
2. H. U. LINDENBERG and H. VORWERK, in Proceedings of the 2nd International Conference on Clean Steel (The Metals Society, Balatonfüred, Hungary, 1981) p. 241.
3. R. RASTOGI and A. W. CRAMB, 84th Steelmaking Conference Proceedings (ISS, Baltimore, 2001), Vol. 28, p. 789.
4. K. SASAI, "Oxygen in Steelmaking: Towards Cleaner Steels" (The Institute of Materials, London, 2001) session 3.1.
5. K. SASAI and Y. MIZUKAMI, *ISIJ Intern.* **41** (2001) 1331.
6. R. J. FRUEHAN, "The Making, Shaping and Treating of Steel" (The AISE Steel Foundation, Pittsburgh, USA, 1998) p. 24.
7. K. SASAI and Y. MIZUKAMI, *ISIJ International* **40** (2000) 40.
8. *Idem.*, *ibid.* **36** (1996) 388.
9. *Idem.*, *ibid.* **38** (1998) 332.
10. E. T. TURKDOGAN, "Fundamental of Steelmaking" (Institute of Materials, Carlton House Terrace, London 1996).
11. J. Y. COGNE, B. HERITIER and J. MONNOT, in Proceedings of the 3rd International Conference on Clean Steel (The Institute of Metals, Balatonfüred, Hungary, 1986).
12. W. TIEKINK and R. KOOTER, "Oxygen in Steelmaking: Towards Cleaner Steels" (The Institute of Materials, London, 2001) session 4.
13. T. B. BRAUN, J. F. ELLIOTT and M. C. FLEMMINGS, *Met. Trans.* **10B** (1979) 171.
14. R. DEKKERS, Doctoral Thesis, Katholieke Universiteit Leuven, Faculteit Wetenschappen, Departement Geografie-Geologie, 2002.
15. H. YIN, H. SHIBATA, T. EMI and M. SUZUKI, *ISIJ Int.* **37** (1997) 936.
16. *Idem.*, *ISIJ International (Japan)* **37** (1997) 946.
17. H. SHIBATA, H. YIN and T. EMI, *Phil. Trans. Royal Soc.* **356A** (1998) 957.
18. H.YIN, H. SHIBATA, T. EMI and J. S. KIM, in Proc. Int. Conf. High Temperature Capillarity (N. Eustathopoulos and N. Sobczak, Krakow, Poland, 1997).
19. Y. WANG, S. SRIDHAR, A. W. CRAMB, A. GOMEZ and C. CICUTTI, *AIST Transactions* (2004) 2, 87.
20. G. ERIKSSON, K. HACK, S. PETERSEN, C. W. BALE, P. CHARTRAND, S. A. DEGTEROV, R. BEN MAHFOUD, J. MELANCON and A. D. PELTON, FactSage Thermochemical Software and Databases .
21. S. KIMURA, Y. NABESHIMA, K. NAKAJIMA and S. MIZOGUCHI, "Belton Memorial Symposium" (Iron and Steel Society, Sydney, Australia, 1998).

Received 31 March
and accepted 20 October 2004